Electronic Supplementary Information

Electronic structures and transport properties of SnS-SnSe nanoribbon lateral heterostructure†

Yang Yang,[ab] Yuhao Zhou,[ab] Zhuang Luo,[a] Yandong Guo,[b] Dewei Rao,*[a] and Xiaohong Yan*[ab]

[a.]School of Materials Science and Engineering, Jiangsu University, Zhenjiang 212013, China. Email: dewei@ujs.edu.cn.
[b.]College of Electronic and Optical Engineering, Nanjing University of Posts and Telecommunications, Nanjing 210046, China. Email: yanxh@ujs.edu.cn.

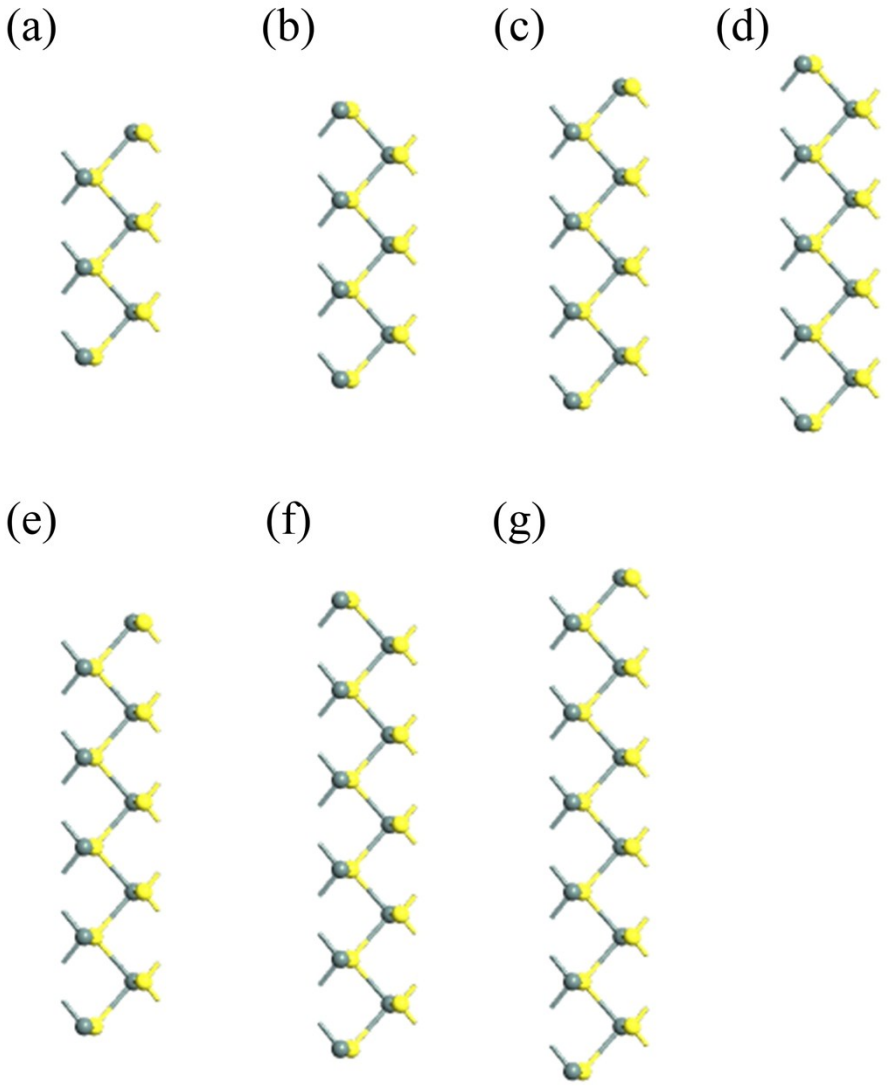

Fig. S1 The unit cell of armchair SnS nanoribbons with different widths. (a) 6A-SnSNR; (b) 7A-SnSNR; (c) 8A-SnSNR; (d) 9A-SnSNR; (e) 10A-SnSNR; (f) 11A-SnSNR; (g) 12A-SnSNR.

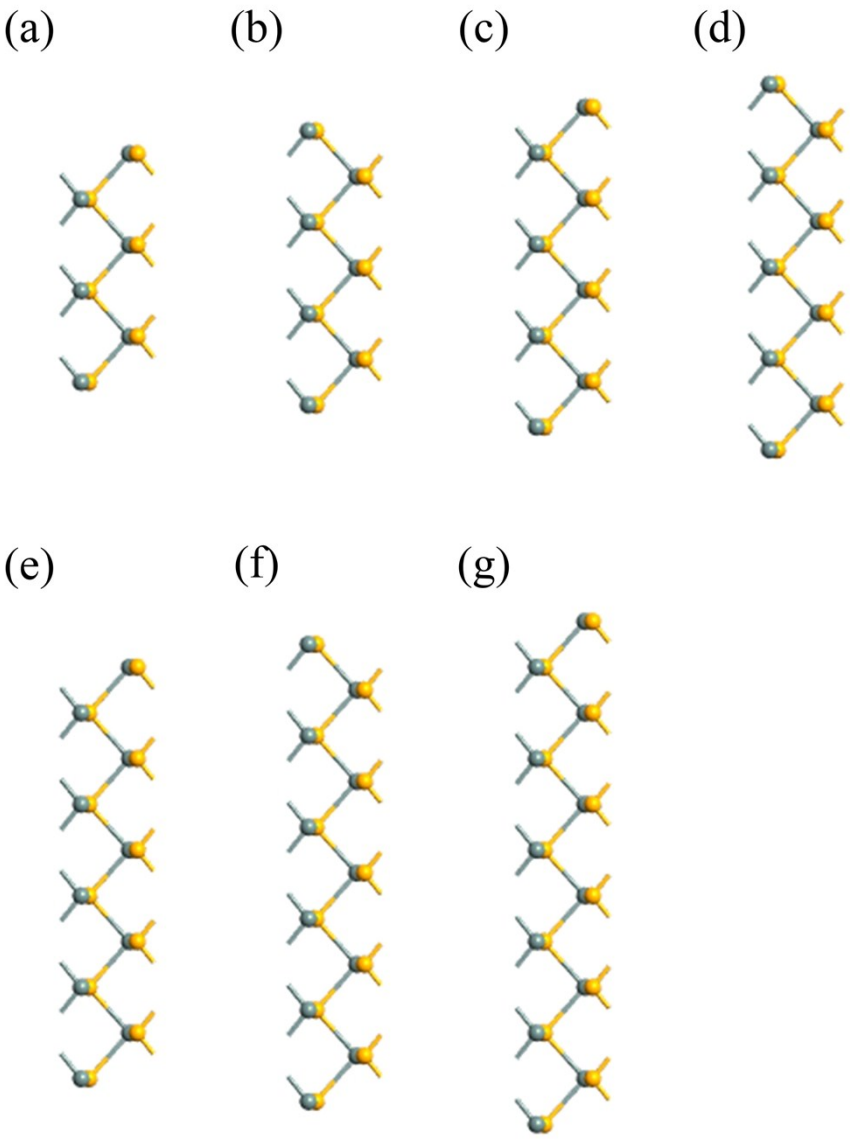

Fig. S2 The unit cell of armchair SnSe nanoribbons with different widths. (a) 6A-SnSeNR; (b) 7A-SnSeNR; (c) 8A-SnSeNR; (d) 9A-SnSeNR; (e) 10A-SnSeNR; (f) 11A-SnSeNR; (g) 12A-SnSeNR.

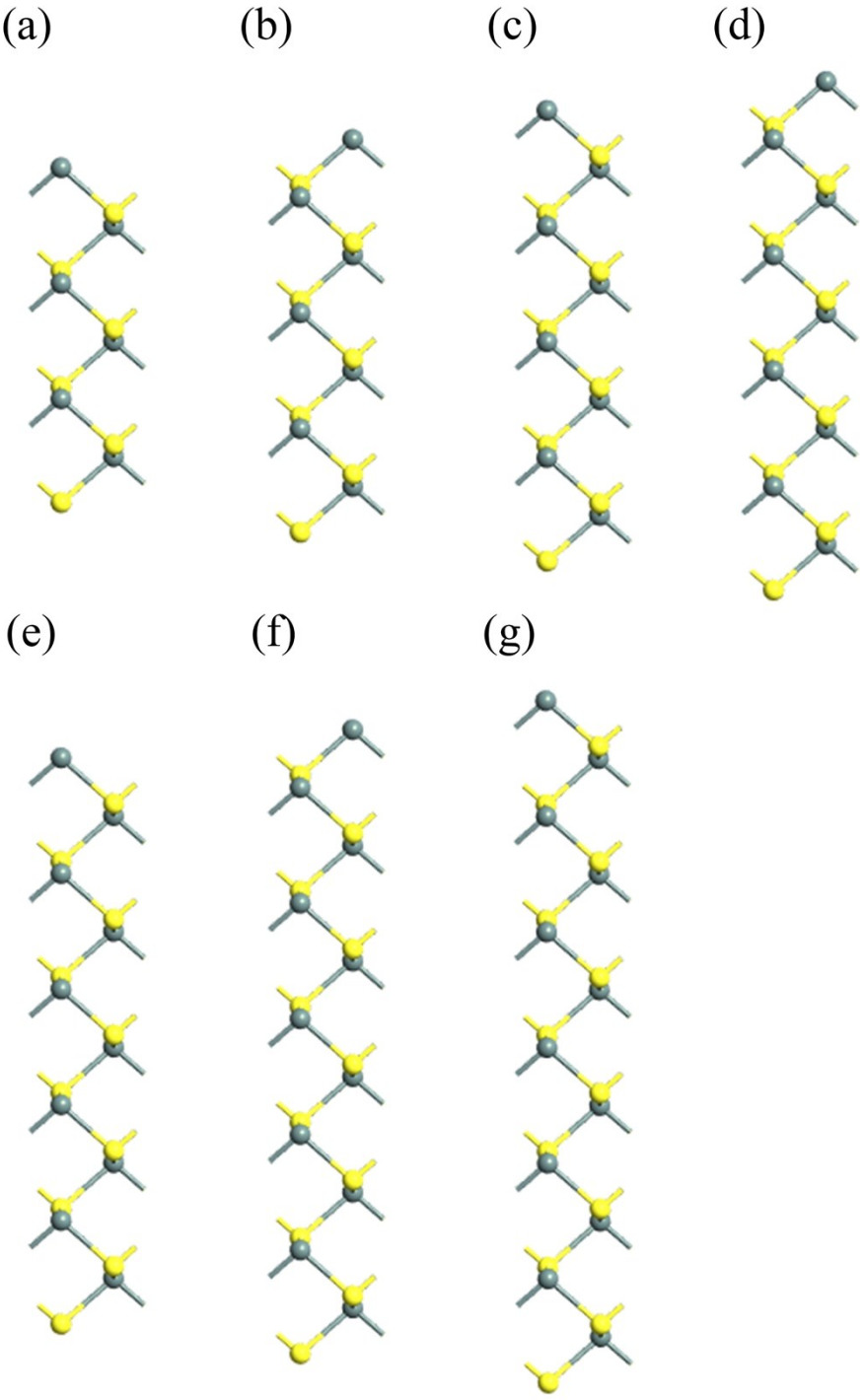

Fig. S3 The unit cell of zigzag SnS nanoribbons with different widths. (a) 6Z-SnSNR; (b) 7Z-SnSNR; (c) 8Z-SnSNR; (d) 9Z-SnSNR; (e) 10Z-SnSNR; (f) 11Z-SnSNR; (g) 12Z-SnSNR.

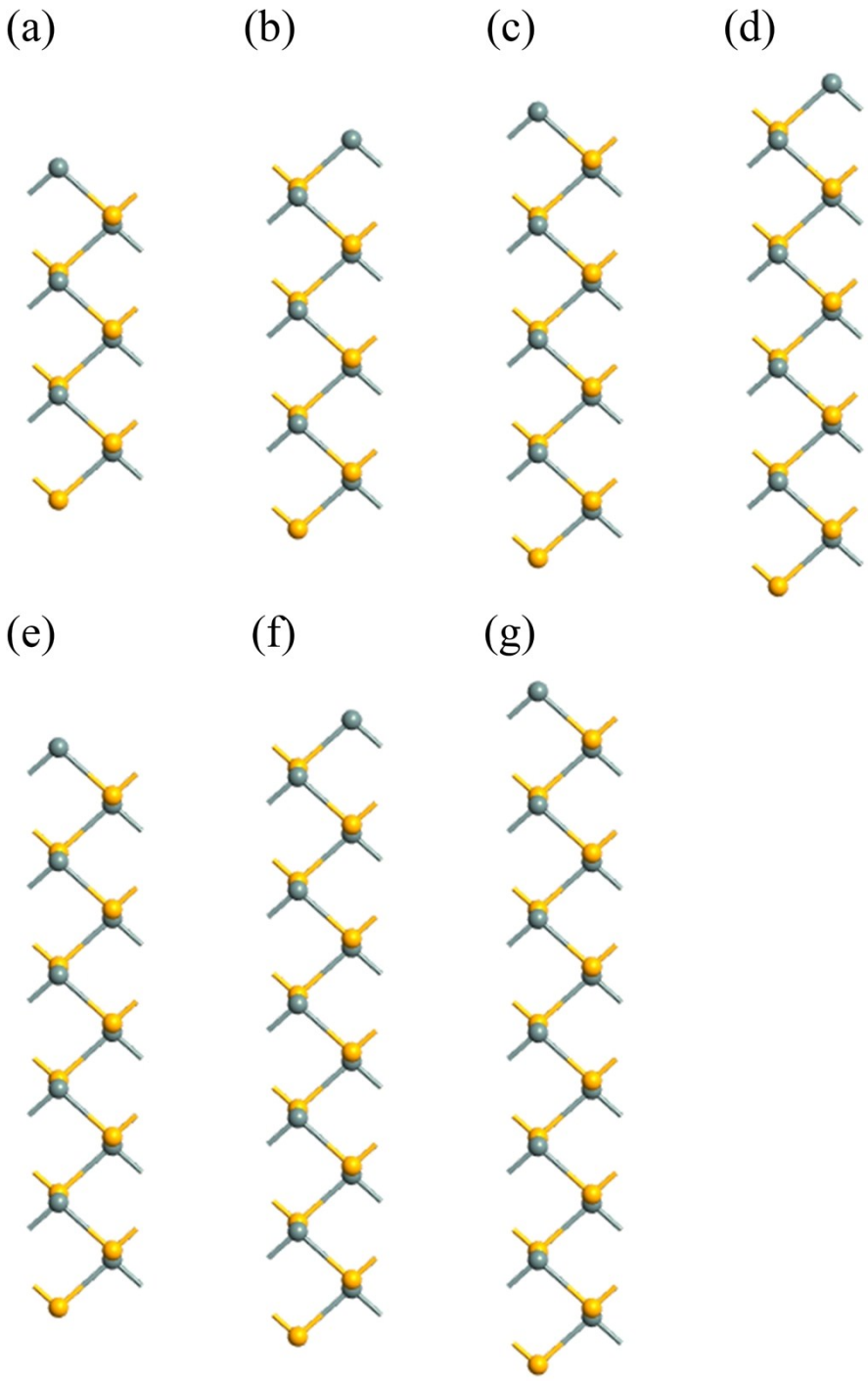

Fig. S4 The unit cell of zigzag SnSe nanoribbons with different widths. (a) 6Z-SnSeNR; (b) 7Z-SnSeNR; (c) 8Z-SnSeNR; (d) 9Z-SnSeNR; (e) 10Z-SnSeNR; (f) 11Z-SnSeNR; (g) 12Z-SnSeNR.

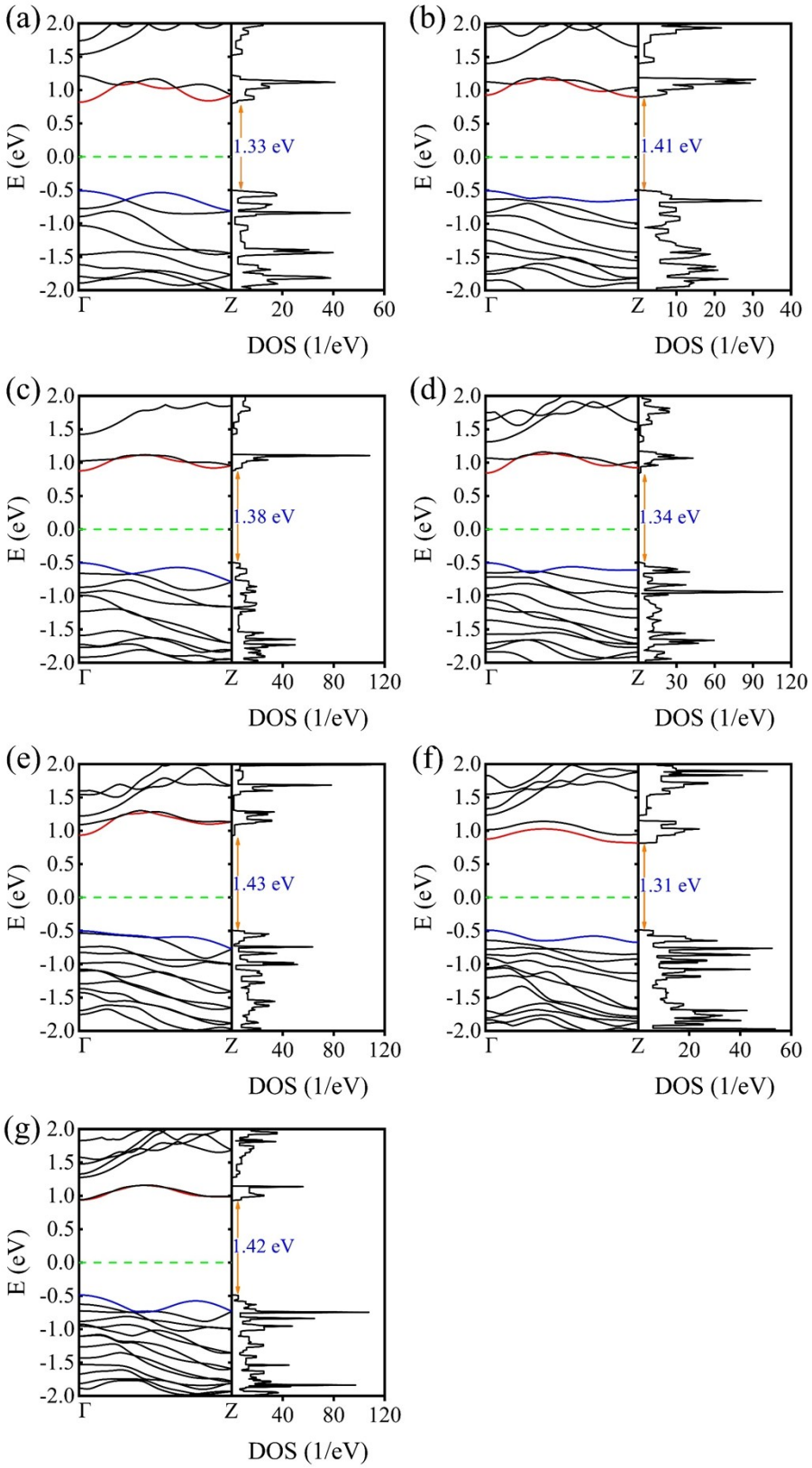

Fig. S5 (a-g) The bandstructures and DOS of 6A-, 7A-, 8A-, 9A-, 10A-, 11A-, and 12A-SnSNR, respectively. The conduction band and valence band are highlighted by red and blue line. The Fermi level is indicated by dashed green line, which has been set to zero.

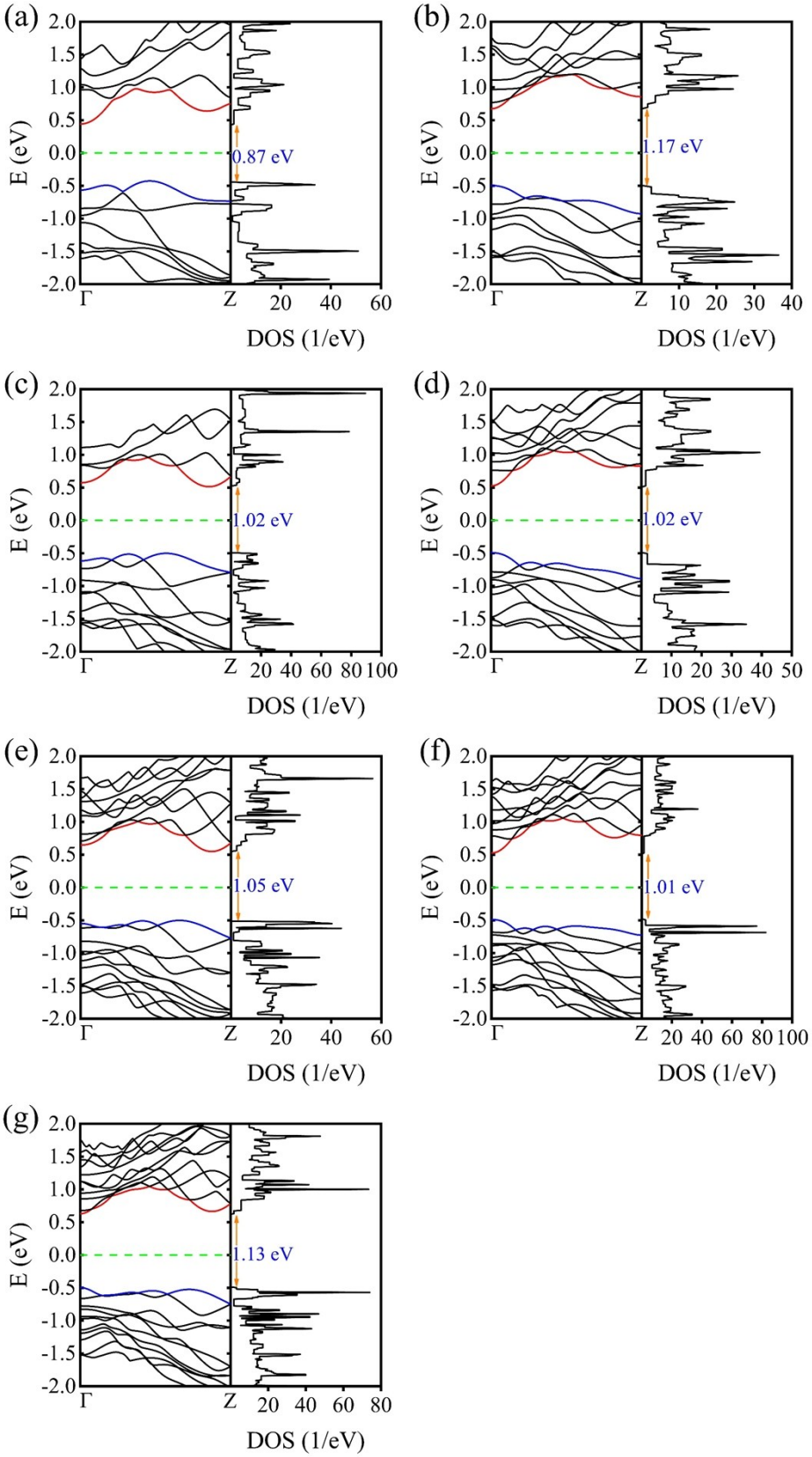

Fig. S6 (a-g) The bandstructures and DOS of 6A-, 7A-, 8A-, 9A-, 10A-, 11A-, and 12A-SnSeNR, respectively. The conduction band and valence band are highlighted by red and blue line. The Fermi level is indicated by dashed green line, which has been set to zero.

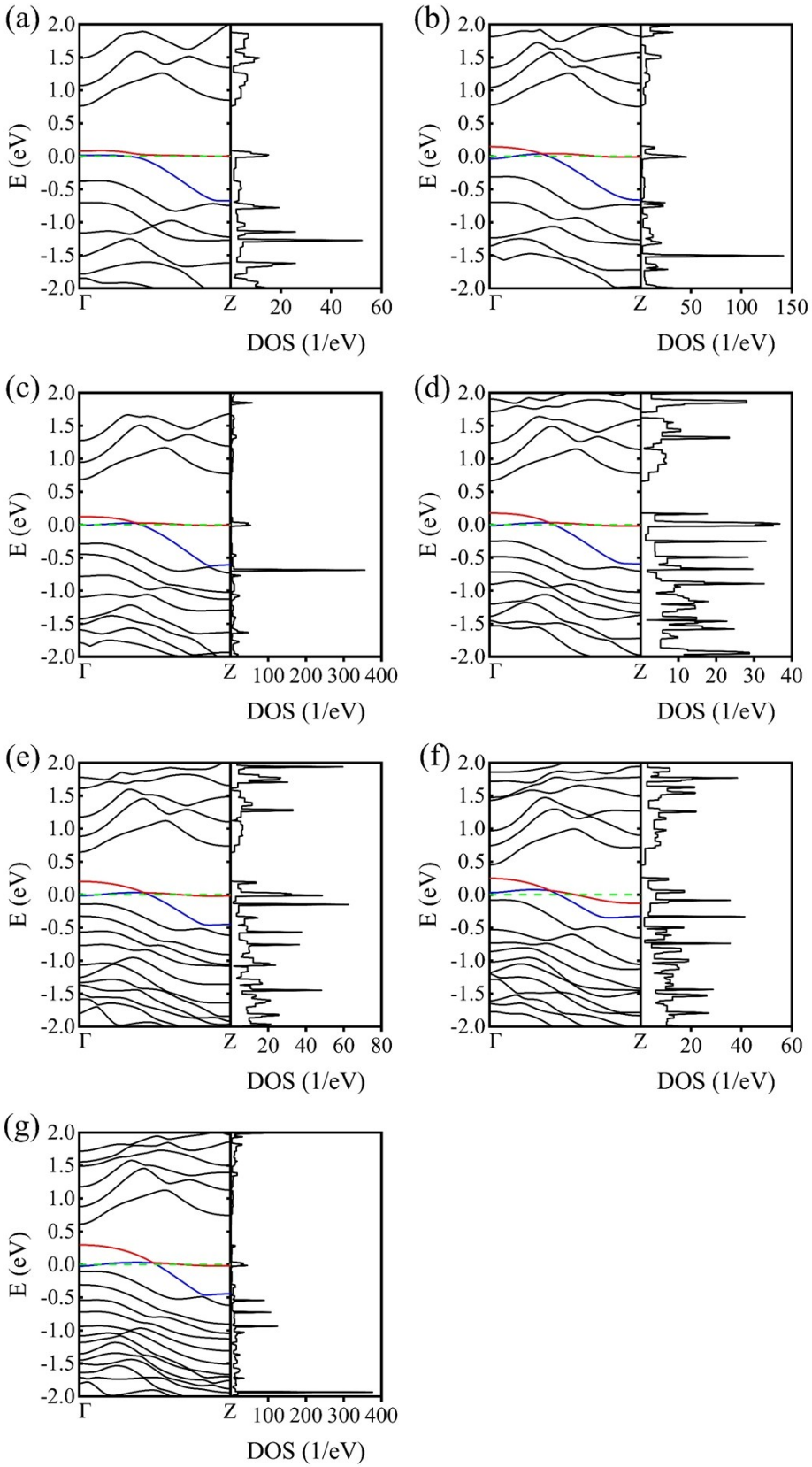

Fig. S7 (a-g) The bandstructures and DOS of 6Z-, 7Z-, 8Z-, 9Z-, 10Z-, 11Z-, and 12Z-SnSNR, respectively. The conduction band and valence band are highlighted by red and blue line. The Fermi level is indicated by dashed green line, which has been set to zero.

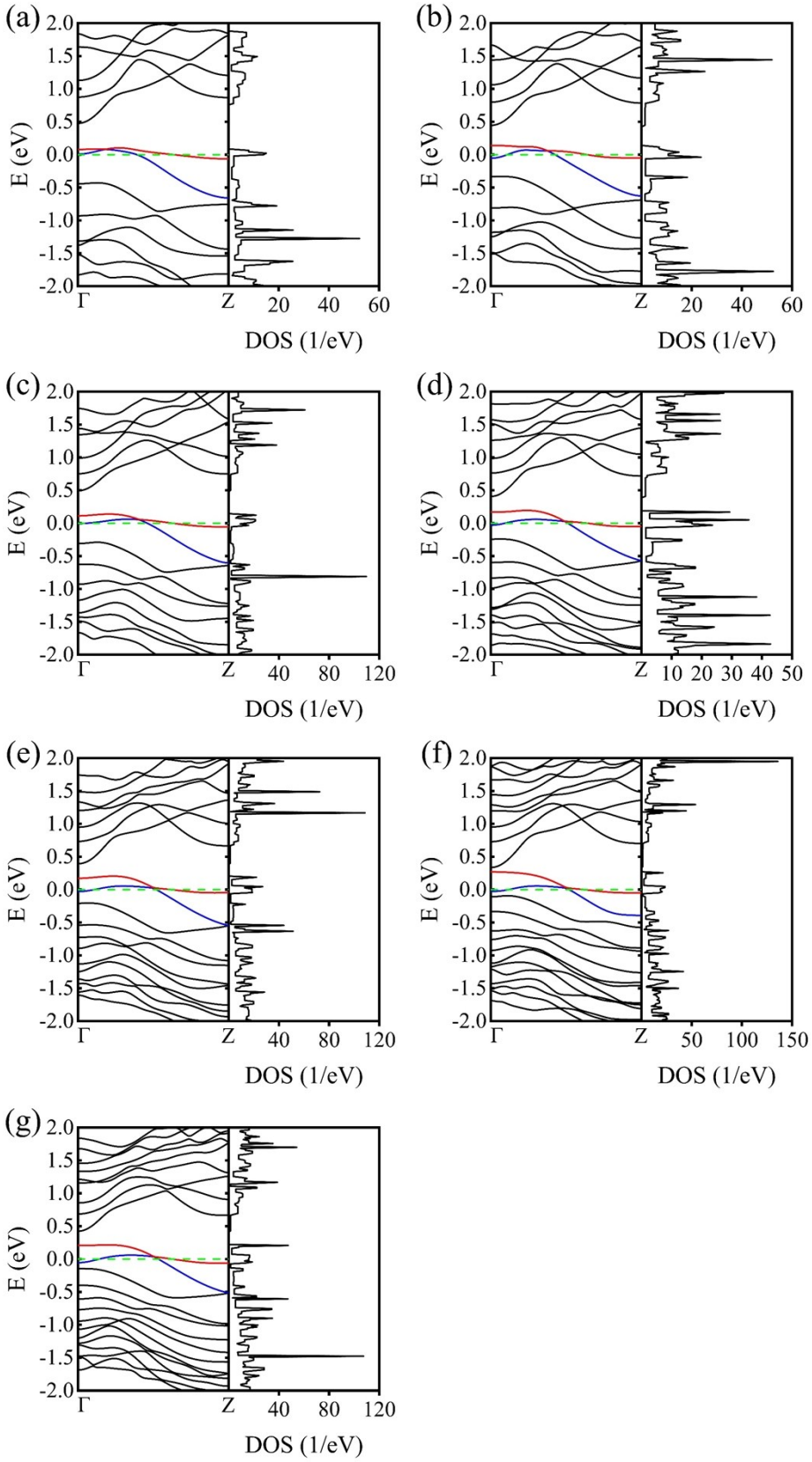

Fig. S8 (a-g) The bandstructures and DOS of 6Z-, 7Z-, 8Z-, 9Z-, 10Z-, 11Z-, and 12Z-SnSeNR, respectively. The conduction band and valence band are highlighted by red and blue line. The Fermi level is indicated by dashed green line, which has been set to

zero.

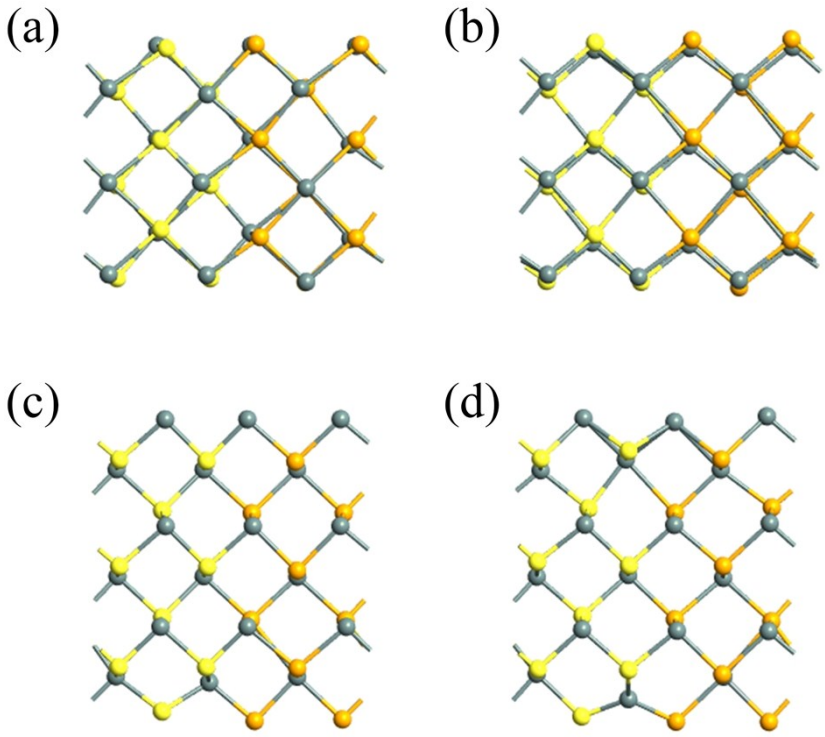

Fig. S9 The interface structures of optimized SnSNR-SnSeNR heterostructures. (a) and (c) 6A-SnSNR-SnSeNR and 6Z-SnSNR-SnSeNR are optimized by ATK. (b) and (d) 6A-SnSNR-SnSeNR and 6Z-SnSNR-SnSeNR are optimized by VASP.

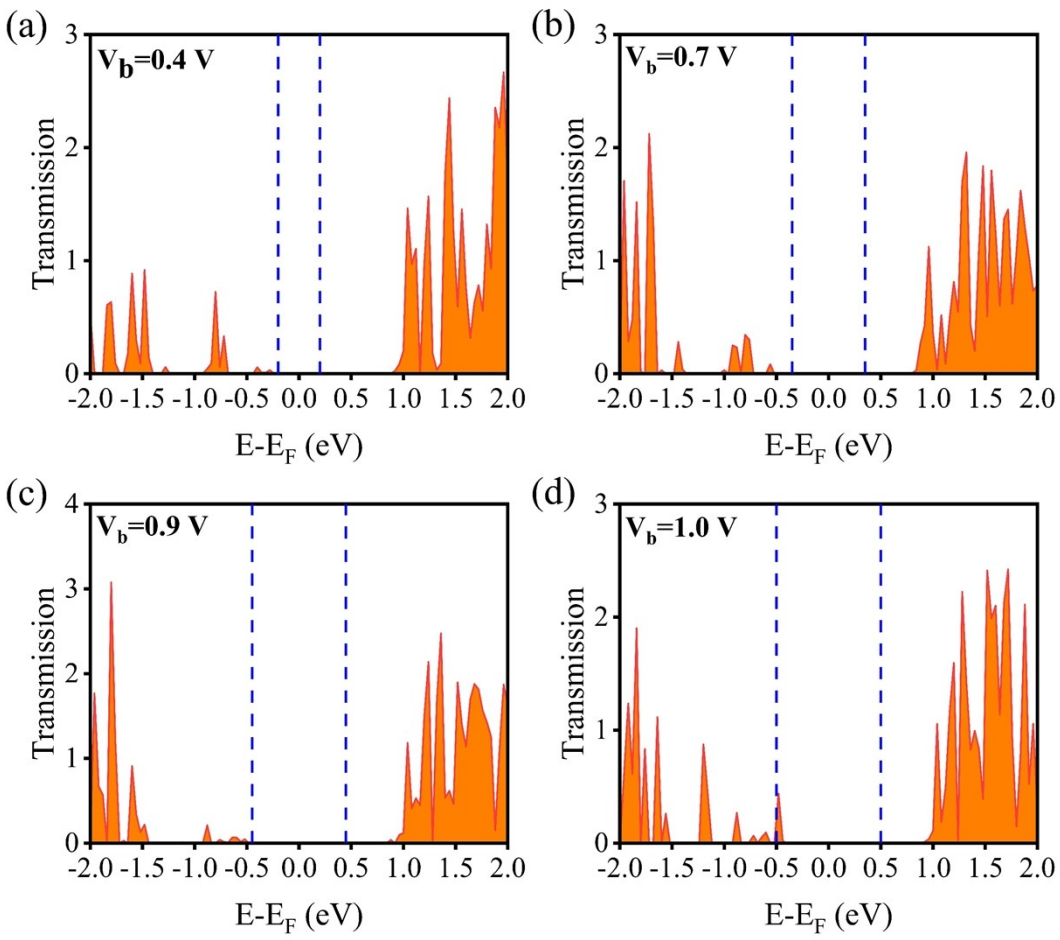

Fig. S10 The bias-dependent transmission spectra of 7A-SnSNR-SnSeNR. (a) 0.4 V, (b) 0.7 V, (c) 0.9 V, (d) 1.0 V. The blue dashed line indicates the bias window.

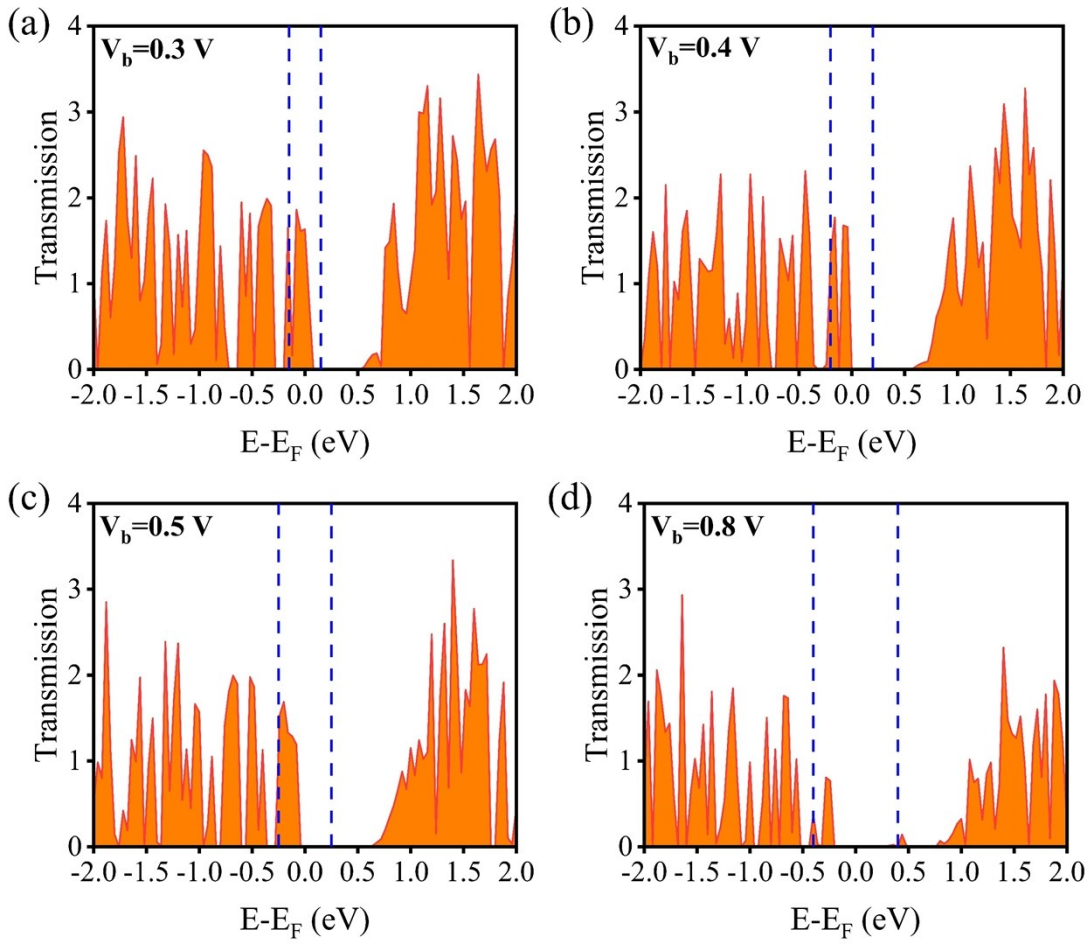

Fig. S11 The bias-dependent transmission spectra of 7Z-SnSNR-SnSeNR. (a) 0.3 V, (b) 0.4 V, (c) 0.5 V, (d) 0.8 V. The blue dashed line indicates the bias window.

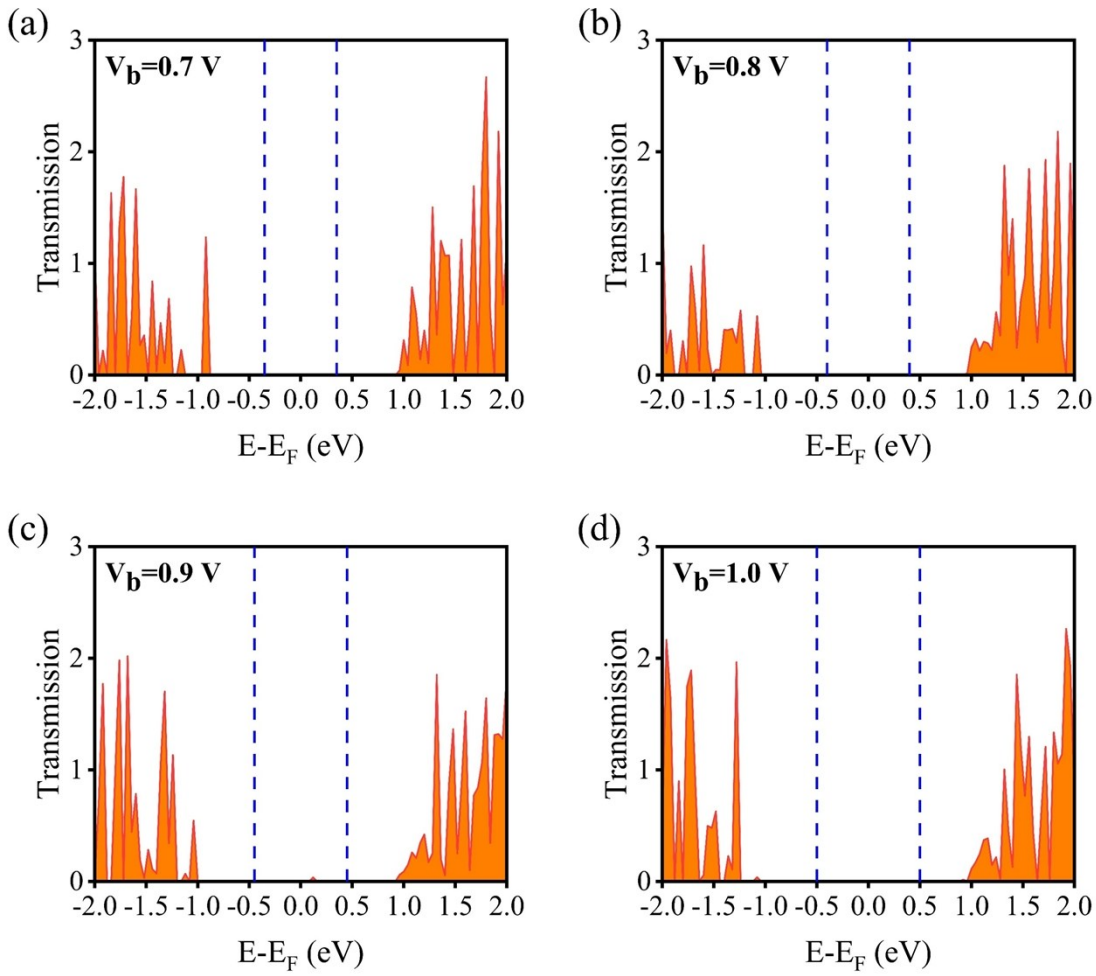

Fig. S12 The bias-dependent transmission spectra of 8A-SnSNR-SnSeNR. (a) 0.7 V, (b) 0.8 V, (c) 0.9 V, (d) 1.0 V. The blue dashed line indicates the bias window.

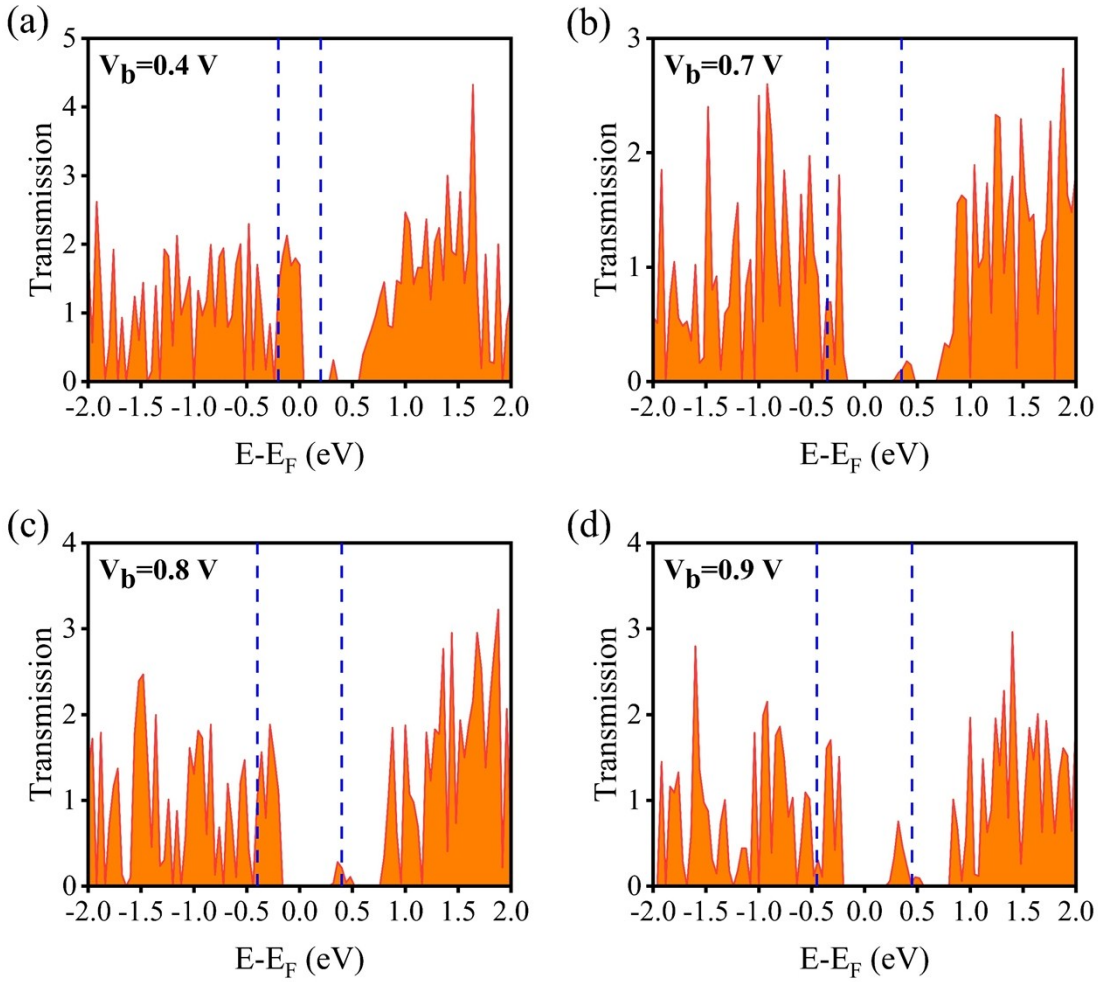

Fig. S13 The bias-dependent transmission spectra of 8Z-SnSNR-SnSeNR. (a) 0.4 V, (b) 0.7 V, (c) 0.8 V, (d) 0.9 V. The blue dashed line indicates the bias window.